Available online at www.sciencedirect.com
SCIENCE DIRECT®
International Journal of Heat and Mass Transfer 48 (2005) 1439–1449
International Journal of HEAT and MASS TRANSFER
www.elsevier.com/locate/ijhmt

Low Reynolds number forced convection in three-dimensional wavy-plate-fin compact channels: fin density effects

Raj M. Manglik [a,*], Jiehai Zhang [a], Arun Muley [b]

[a] Thermal-Fluids and Thermal Processing Laboratory, Department of Mechanical, Industrial and Nuclear Engineering, University of Cincinnati, 598 Rhodes Hall, P.O. Box 210072, Cincinnati, OH 45221-0072, USA
[b] Honeywell Engines, Systems and Services, Torrance, CA 90504, USA

Received 6 July 2004; received in revised form 29 October 2004
Available online 19 December 2004

Abstract

Steady forced convection in periodically developed low Reynolds number ($10 \leqslant Re \leqslant 1000$) air ($Pr = 0.7$) flows in three-dimensional wavy-plate-fin cores is considered. Constant property computational solutions are obtained using finite-volume techniques for a non-orthogonal non-staggered grid. Results highlight the effects of wavy-fin density on the velocity and temperature fields, isothermal Fanning friction factor f, and Colburn factor j. The fin waviness is seen to induce the steady and spatially periodic growth and disruption of symmetric pairs of counter-rotating helical vortices in the wall-trough regions of the flow cross-section. The thermal boundary layers on the fin surface are thereby periodically interrupted, resulting in high local heat transfer near the recirculation zones. Increasing fin density, however, tends to dampen the recirculation and confine it. The extent of swirl increases with flow rate, when multiple pairs of helical vortices are formed. This significantly enhances the overall heat transfer coefficient as well as the pressure drop penalty, when compared to that in a straight channel of the same cross-section. The relative surface area compactness as measured by the (j/f) performance or the area goodness factor nevertheless increases with fin density.

1. Introduction

Forced convective heat transfer between gas and liquid streams is commonly encountered in heat exchangers used in the automotive and climate control (heating, cooling, air conditioning and refrigeration) applications. Generally plate-fin type exchangers are used, where the air- or gas-side convection coefficient is a small fraction (5–20%) of that on the liquid side [1–3], thus constituting the controlling thermal resistance in the exchangers. Extended surfaces or fins in a variety of geometries are often used to mitigate this problem and enhance the heat transfer. Besides increasing the effective surface area, enhanced-fin cores made up of offset-strip fins, louvered fins, perorated fins, and corrugated or wavy fins, among others, also improve the heat transfer coefficient by altering the flow field [1–6]. Of these, wavy fins are particularly attractive for their simplicity of manufacture, potential for enhanced thermal-hydraulic performance, and ease of use in both plate-fin and tube-fin type exchangers.

A typical wavy plate-fin core, formed by placing wavy fins side-by-side and bonding them to a set of flat

* Corresponding author. Tel.: +1 513 556 5704; fax: +1 513 556 3390.
E-mail address: raj.manglik@uc.edu (R.M. Manglik).

0017-9310/$ - see front matter © 2004 Elsevier Ltd. All rights reserved.
doi:10.1016/j.ijheatmasstransfer.2004.10.022

Nomenclature

A	amplitude (m), and surface and/or cross-sectional area (m^2)
B	dimensionless pressure gradient, Eq. (3b)
Br	Brinkman number ($=\mu u_m/k\Delta T$)
c_p	specific heat (J/kg K)
d_h	hydraulic diameter (m)
f	Fanning friction factor
j	Colburn factor ($=Nu/RePr^{1/3}$)
H	fin height (m)
H1	uniform heat flux with constant peripheral wall temperature boundary condition
h	heat transfer coefficient (W/m^2K)
k	thermal conductivity (W/m K)
L	pitch of fin waviness (m)
$\dot{m}$	mass flow rate (kg/s)
Nu	Nusselt number ($=hd_h/k$)
Pr	Prandtl number ($=\mu c_p/k$)
p	pressure (Pa)
p^*	local pressure (Pa)
q''_w	wall heat flux (W/m^2)
Re_S	Reynolds number based on fin spacing ($=Su_m/v$)
Re	Reynolds number based on hydraulic diameter ($=d_hu_m/v$)
S	fin spacing (m)
T	temperature (K)
T	uniform wall temperature boundary condition
U, V, W	dimensionless velocity components
u, v, w	x-, y-, and z-velocity components (m/s)
x, y, z	Cartesian coordinates

Greek symbols

Γ	dimensionless coefficient, Eq. (7a)
α	duct cross-section aspect ratio ($=S/H$)
β	global pressure gradient (Pa/m)
ε	channel or fin spacing ratio ($=S/2A$)
γ	fin-plate waviness or corrugation ratio ($=2A/L$)
μ	dynamic viscosity (Pa s or $N s/m^2$)
θ	dimensionless temperature
ρ	density (kg/m^3)
ω	geometrical parameter, Eq. (2b)
ξ, η, ζ	body-fitted coordinates

Subscripts

c	pertaining to cross-section area
b	bulk value
H	pertaining to the uniform heat flux boundary condition
m	mean or average value
pf	plain fin or flat plate
s	pertaining to surface area
T	pertaining to the uniform wall temperature boundary condition
w	at wall conditions
wf	wavy fin or wavy plate

plates, is illustrated in Fig. 1(a) and (b). The geometrical features of the three-dimensional inter-fin flow channel shown in Fig. 1(c) are described by the fin height H, fin spacing S, amplitude of waviness A, and wavelength or pitch of waviness L. The dimensionless representations of these variables are given by the fin-spacing ratio ($\varepsilon = S/2A$), flow cross-section aspect ratio ($\alpha = S/H$), and corrugation or waviness aspect ratio ($\gamma = 2A/L$). For a given fin height and waviness, ε and α also represent the fin density (ε and α decrease with increasing fin density but fixed A and H). It may further be noted that while a sinusoidal profile for the fin waviness is depicted and considered in this study, other shapes (triangular or trapezoidal) are also possible [4].

A two-dimensional representation of the wavy-plate-fin core as a parallel-corrugated-plate channel with heat transfer at the wavy walls, which is an idealization of and quite different from the three-dimensional model of Fig. 1, has been considered in much of the earlier literature. Nevertheless, the results are instructive and the flow behavior is found to be characterized by the generation of lateral swirl or fluid recirculation in the trough

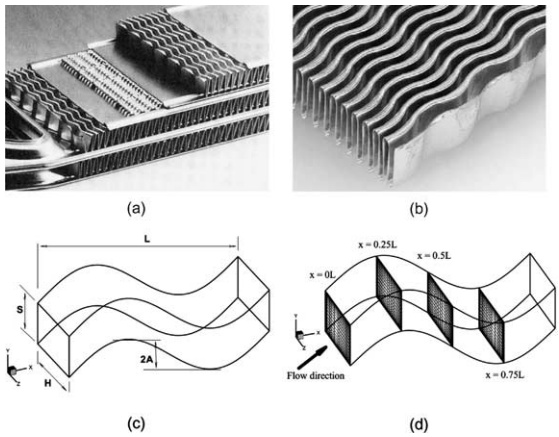

Fig. 1. Geometrical description of three-dimensional sinusoidal wavy-plate-fin channel: (a) Typical wavy-plate-fin cross-flow heat exchanger core, (b) enlarged view of a wavy-fin geometry, (c) characteristic dimensions of a wavy-fin channel, and (d) flow cross-section grid location markers along the axial length of one-period duct module.

regions of the wavy channels. The consequent periodic thinning and disruption of the boundary layers produces significant enhancement of heat and mass transfer [7–20]. This body of literature has primarily addressed the steady-state forced convective characteristics of wavy-wall channels, albeit as a simplified model, in several different applications that include plate-fin exchangers [7–12], tube-fin cores [13–15], blood oxygenators [16,17], and gasketted plate-and-frame heat exchangers [18–20], among others [21,22].

Asako and Faghri [7] have numerically investigated two-dimensional steady laminar flow ($100 \leqslant Re \leqslant 1000$) and heat transfer in plate channels with triangular-profiled wall corrugations that are maintained at a uniform temperature. Subsequently, triangular corrugations with rounded corners were considered [8], and the consequent change in heat transfer rates was found to depend on the specific flow conditions, geometry, and performance constraints. The nature and convective influence of recirculation cells that are formed in the troughs of sinusoidal wall corrugations have also been explored in two previous studies [12,20]. Zhang et al. [12] have numerical investigated the effects of wall-corrugation aspect ratios ($0.125 \leqslant \gamma \leqslant 0.5$) and fin spacing ratios ($0.1 \leqslant \varepsilon \leqslant 3.0$) on the vortex structure and enhanced heat transfer for flow rates with $Re = 10$–1000. Likewise, Metwally and Manglik [20] have investigated two-dimensional periodically developed laminar flow and heat transfer in sinusoidal wavy channels with fin spacing ratio $\varepsilon = 1$, and corrugation aspect ratios $0.25 \leqslant \gamma \leqslant 1.0$. As seen from the results of these studies [7–10,12,20], the axial flow gets separated downstream of the wall-corrugation peaks and re-attaches upstream of the subsequent wall peak, thereby encapsulating a lateral vortex in the trough region. The strength of recirculation and extent of its spatial coverage increase with Re, γ and ε, leading to substantially enhanced momentum and energy transport.

Steady-state laminar forced convection in the complete three-dimensional flow geometry of the wavy-fin cores has received scant attention in the literature. The earliest experimental data, though rather limited, are given in the classical Kays and London [2] sourcebook, and little has since been done to supplement them [3–6]. Three-dimensional numerical simulations of laminar air flow ($100 \leqslant Re \leqslant 2000$) heat transfer in sinusoidal wavy flow channels that have a trapezoidal cross-section have been carried out by Asako et al. [23]. Some results with channel spacing ratios of $\varepsilon = 0.25$ and 0.5 have been obtained that show helical flow recirculation and local mixing in the wavy-wall troughs. This work was extended by Utriainen and Sundén [24] with a limited analysis of cross-corrugated trapezoidal-profiled channels. Subsequently, they [25] have also considered wavy cores with rounded-corner triangular profiles, and their computational results indicate enhanced thermal-hydraulic performance due to helical secondary flow in each wall-wave trough module. More complex three-dimensional, cross-corrugated flow channels have also been computationally modeled in a few recent studies [26,27].

Table 1
List of geometrical attributes of four wavy-fin cores considered in the computational simulations

Wavy-fin core	Cross-section aspect ratio α (=S/H)	Fin waviness ratio γ (=$2A/L$)	Fin separation ratio ε (=$S/2A$)
Case 1	0.968	0.2667	1.220
Case 2	0.637	0.2667	0.803
Case 3	0.373	0.2667	0.470
Case 4	0.240	0.2667	0.303

The design and application of rectangular sinusoidal wavy-plate fins in compact heat exchangers requires a more specific and detailed assessment of their thermal-hydraulic performance, which is addressed in this paper. Steady forced convection in air flow ($Pr = 0.7$) in the laminar or low Reynolds number regime ($10 \leqslant Re \leqslant 1000$) is computationally investigated. For the heating/cooling of the flat surfaces (the wall interface between two fluid streams in a plate-fin exchanger; Fig. 1c), two different thermal conditions are considered: (a) constant wall temperature, which is typical of refrigerant-air or liquid-air exchangers, and (b) constant wall heat flux, which is normally encountered with equal heat capacity air/gas-to-air/gas or liquid-to-liquid fluid streams. The parametric effects of channel spacing ratio ε and cross-section aspect ratio α, both of which are dictated by the wavy-fin density for a fixed height, are delineated; the four different cases considered in this study are listed in Table 1. The character of helical swirl flow patterns in a wavy-fin module and their influence on the heat transfer are outlined, along with an evaluation of the enhanced performance relative to straight rectangular channels.

2. Mathematical formulations

For the coordinate system and fin-channel geometry shown in Fig. 1(c) and 1(d), the computational model considers a one-period-long sinusoidal wavy channel with periodically developed flow conditions. For computational convenience, the following generalized dimensionless body-fitted coordinates are applied to transform the physical domain (x, y, z) onto a cuboidal (ξ, η, ζ) domain:

$$\xi = (x/S), \quad \eta = [(y/S) - (A/S)\sin(2\pi S\xi/L)], \quad \zeta = (z/S) \tag{1}$$

The laminar ($10 \leqslant Re \leqslant 1000$) air ($Pr = 0.7$) flow field is characterized by steady state, constant property conditions, with negligible axial conduction ($Pe \gg 1$)

and viscous dissipation ($Br \ll 1$). It may be noted here that while some investigators [11,28] have contended that steady-state conditions may not exist as $Re \to 1000$, several others [23–26] have considered steady flows in their three-dimensional computations. In fact, such has been the case in many other instances where convection is characterized be helical flows [29–32]. Also, there is some empirical evidence [19,22,33] to justify the steady-state assumption in the present analysis, and the assessment of when instability sets in is beyond its scope.

In the computational (ξ, η, ζ) domain, the dimensionless velocity components (U, V, W) are given by

$$U = (u/u_m), \quad V = [(v/u_m) - \omega U], \quad W = (w/u_m) \tag{2a}$$

where u_m is the mean axial velocity, and

$$\omega = (2\pi A/L)\cos(2\pi S\xi/L) \tag{2b}$$

Also, for periodically developed flows, the pressure field can be decomposed into its two constituent parts and expressed as

$$p(x,y,z) = [p^*(x,y,z) - \beta x] \tag{3a}$$

Here β is the constant global pressure gradient that drives the axial flow and p^* is the local pressure that exhibits periodicity and the cause of local variations in the flow field. Their respective dimensionless forms are

$$B = (\beta S/\rho u_m^2), \quad P = (p^*/\rho u_m^2) \tag{3b}$$

With the flow channel walls subjected to (a) the uniform wall temperature boundary condition, which typically models the heat transfer condition in refrigerant-to-air evaporators and condensers as well as in many liquid-to-air recuperators, and (b) the uniform wall heat flux condition to model gas/liquid-to-gas/liquid compact exchangers, the respective dimensionless temperatures can be defined as

$$\theta_T(x,y,z) = \{[T(x,y,z) - T_w]/[T_b(x) - T_w]\} \tag{4a}$$

$$\theta_H(x,y,z) = \left[\frac{T(x,y,z) - T_{ref}}{q''_w S/k} - \frac{d(T(x)_b - T_w)/d\xi}{(T_b(x) - T_w)q''_w S/kx}\right] \tag{4b}$$

In this expression, $T_b(x)$ is the local bulk or mixed-mean temperature that is given by its usual definition

$$T_b(x) = \left[\int\int |u| T(x,y,z)\,dy\,dz \Big/ \int\int |u|\,dy\,dz\right] \tag{5}$$

and the dimensionless θ_T and θ_H explicitly satisfy the periodic boundary condition over the inlet and outlet of the one-period computational flow domain.

With the introduction of these variables, the governing transport equations can thus be restated in dimensionless forms, and the mass conservation equation can be expressed as

$$\frac{\partial U}{\partial \xi} + \frac{\partial V}{\partial \eta} + \frac{\partial W}{\partial \zeta} = 0 \tag{6}$$

Whereas the momentum and energy transport equations can be written in the following generalized form:

$$U\frac{\partial \phi}{\partial \xi} + V\frac{\partial \phi}{\partial \eta} + W\frac{\partial \phi}{\partial \zeta} = \Gamma\left[\frac{\partial^2 \phi}{\partial \xi^2} + (1+\omega^2)\frac{\partial^2 \phi}{\partial \eta^2} + \frac{\partial^2 \phi}{\partial \zeta^2}\right] + S_\phi \tag{7a}$$

Here $\phi = U$, V, W, and θ for the three dimensionless velocity components and temperature, respectively, and $\Gamma = (1/Re_S)$ for the momentum equations, and $[1/(Re_S Pr)]$ for the energy equation. Also, the respective source terms S_ϕ are expressed as follows:

$$S_U = -\frac{1}{Re_S}\left[\frac{\partial}{\partial \xi}\left(\omega\frac{\partial U}{\partial \eta}\right) + \omega\frac{\partial}{\partial \eta}\left(\frac{\partial U}{\partial \xi}\right)\right] + B - \frac{\partial P}{\partial \xi} + \omega\frac{\partial P}{\partial \eta} \tag{7b}$$

$$S_V = -\frac{1}{Re_S}\left[\frac{\partial}{\partial \xi}\left(\omega\frac{\partial V}{\partial \eta}\right) + \omega\frac{\partial}{\partial \eta}\left(\frac{\partial V}{\partial \xi}\right)\right] + \omega\frac{\partial P}{\partial \xi} - (1+\omega^2)\frac{\partial P}{\partial \eta} + \frac{1}{Re_S}\left[2\frac{\partial \omega}{\partial \xi}\left(\frac{\partial U}{\partial \xi} - \omega\frac{\partial U}{\partial \eta}\right) + U\frac{\partial^2 \omega}{\partial \xi^2}\right] - \omega B - U\frac{\partial^2 \omega}{\partial \xi} \tag{7c}$$

$$S_W = -\frac{1}{Re_S}\left[\frac{\partial}{\partial \xi}\left(\omega\frac{\partial W}{\partial \eta}\right) + \omega\frac{\partial}{\partial \eta}\left(\frac{\partial V}{\partial \xi}\right)\right] - \frac{\partial P}{\partial \zeta} \tag{7d}$$

$$S_{\theta_T} = -\frac{1}{Re_S Pr}\left[\frac{\partial}{\partial \xi}\left(\omega\frac{\partial \theta_T}{\partial \eta}\right) + \omega\frac{\partial}{\partial \eta}\left(\frac{\partial \theta_T}{\partial \xi}\right)\right] + \left[\frac{2}{Re_S Pr}\left(\frac{\partial \theta_T}{\partial \xi} - \omega\frac{\partial \theta_T}{\partial \eta}\right) - U\theta_T\right]\left(\frac{d(T_b - T_w)/d\xi}{T_b - T_w}\right) + \frac{\theta_T}{Re_S Pr}\left[\left(\frac{d(T_b - T_w)/d\xi}{T_b - T_w}\right)^2 + \frac{d}{d\xi}\left(\frac{d(T_b - T_w)/d\xi}{T_b - T_w}\right)\right] \tag{7e}$$

$$S_{\theta_H} = -\frac{1}{Re_S Pr}\left[\frac{\partial}{\partial \xi}\left(\omega\frac{\partial \theta_H}{\partial \eta}\right) + \omega\frac{\partial}{\partial \eta}\left(\frac{\partial \theta_H}{\partial \xi}\right)\right] - \left[U\frac{d(T_b - T_w)/d\xi}{(T_b - T_w)q''_w/k}\right] \tag{7f}$$

Furthermore, U, V, W, and θ in these equations explicitly satisfy the no-slip, thermal boundary (T_w = constant or q''_w = constant), and periodicity conditions, where the inlet–outlet periodicity in the one-module flow domain (Fig. 1c) essentially requires that

$$\phi(U,V,W,\theta)_{\xi=0} = \phi(U,V,W,\theta)_{\xi=1} \tag{8}$$

With the flow distribution given by the solution for Eqs. (6) and (7), the period-averaged isothermal Fanning friction factor for the periodically developed conditions is obtained from its usual definition as

$$f = -[(\mathrm{d}p/\mathrm{d}x)(d_h/2\rho u_m^2)] = (Bd_h/2S) \tag{9}$$

Also, the overall period-averaged Nusselt number is computed from the energy balance over the one-period flow domain, and the log-mean temperature difference (ΔT_{lm}) as

$$\mathrm{Nu} = \frac{\dot{m}c_p(T_{b,\xi=1} - T_{b,\xi=0})d_h}{kA_s\Delta T_{lm}} = (A_c/A_s)(Re\,Pr)\left[-\int_0^L \frac{\mathrm{d}(T_b - T_w)/\mathrm{d}\xi}{T_b - T_w}\,\mathrm{d}x\right] \tag{10a}$$

where

$$\Delta T_{lm} = \frac{(T_w - T_{b,\xi=1}) - (T_w - T_{b,\xi=0})}{\ln[(T_w - T_{b,\xi=1})/(T_w - T_{b,\xi=0})]} \tag{10b}$$

The heat transfer results, however, are presented in terms of the Colburn j factor ($Nu/Re\,Pr^{1/3}$), in conformity with the customary design and engineering practice in the compact heat exchanger literature [2–4,6].

3. Numerical solution

To obtain numerical solutions, the governing differential equations were discretized using the finite-volume method on a structured, non-orthogonal grid. The computational mesh for the flow geometry is uniform in the axial x or ξ direction, but non-uniform in the cross-sectional plane, i.e., y or η and z or ζ directions. The latter non-uniform mesh distribution is controlled by the following functions:

$$\eta = ay_1 + (1-a)\frac{1-\tanh[b(1-y_1)}{\tanh(b)}$$
$$\zeta = ay_2 + (1-a)\frac{1-\tanh[b(1-y_2)}{\tanh(b)} \tag{11}$$

Here y_1 and y_2 have a uniform distribution in the range $0 \leqslant (y_1, y_2) \leqslant 1$, and the η- and ζ-distributions in the range $0 \leqslant (\eta, \zeta) \leqslant 1$ are controlled be the two constant that were set as $a = 0.1$, and $b = 2.0$ in all simulations. This ensures a denser mesh near the walls for properly treating the high velocity and temperature gradients. Both the diffusion and convection terms are treated by the power-law scheme, [1] and central differencing is applied to the source terms. The SIMPLE algorithm [34] evaluates the coupling between pressure and velocity. Also, for the periodically developed flow condition as treated by Patankar et al. [35] and others, the inlet–outlet periodicity of the flow velocity components and temperature is explicitly imposed over a single corrugation module L in the stream-wise direction as given by Eq. (8). The local bulk-mean temperature is obtained from its general definition in Eq. (5), where the numerical integration is performed by a second-order accurate scheme. The mean velocity or flow Reynolds number is an a priori input, and the pressure gradient determined iteratively to satisfy the momentum conservation equations. More details of the computational methodology using an in-house developed code and grid representation can be found in Ref. [21].

The grid selection was made after selective successive grid refinement experiments, where the final mesh resulted in less than 0.2% change in the computed values of f and j. For example, for the Case 1 (Table 1) wavy fin channel with $\alpha = 0.968$, $\gamma = 0.2667$, and $\varepsilon = 1.22$, and a flow rate of $Re = 500$, the f and j simulation results for five different mesh sizes are listed in Table 2, where it can be seen that the relative error decreases with successive mesh refinement to $\leqslant$0.2%. Similar grid refinement experiments were carried out for other cases as well. In all computations, the convergence criteria were set such that the residual was less that 10^{-6} for each of velocity, pressure, and temperature. Further validation of numerical results was obtained by comparing them with the analytical solutions for straight rectangular channels and one set of experimental data [33]. When the channel amplitude A is set to zero, straight rectangular flow channels are obtained, and their analytical results for (fRe) and Nu can be found in Ref. [36]. For example, in a straight rectangular duct of cross-section aspect ratio $\alpha = 0.968$ (Case 1, $A \to 0$), the computed value of (fRe) = 14.32 and $Nu = 2.961$ were within ±1% of the

Table 2
Effect of grid size on f and j results in a typical wavy-fin channel (Case 1) with $\alpha = 0.968$, $\gamma = 0.2667$, and $\varepsilon = 1.220$, for air ($Pr = 0.7$) flow rate of $Re = 500$

Grid size ($\xi \times \eta \times \zeta$)	Number of nodes	Friction factor f	Colburn factor j
$50 \times 21 \times 21$	22,050	0.20392	0.02115
$60 \times 25 \times 25$	37,500	0.20896 (+2.47%)[a]	0.02249 (+6.34%)[a]
$70 \times 31 \times 31$	67,270	0.21079 (+0.88%)	0.02302 (+2.36%)
$80 \times 35 \times 35$	98,000	0.21164 (+0.40%)	0.02326 (+1.04%)
$90 \times 41 \times 41$	151,290	0.21197 (+0.16%)	0.02331 (+0.21%)

[a] Relative error based on the result of previous coarser mesh.

[1] This obviates the need to track local Peclet number Pe, as it is valid and accurate over the entire range of Pe that would be encountered in the corrugated duct swirl flow regime, and is not hampered by the narrow-range restrictions for upwind, central-differencing, or hybrid schemes [34].

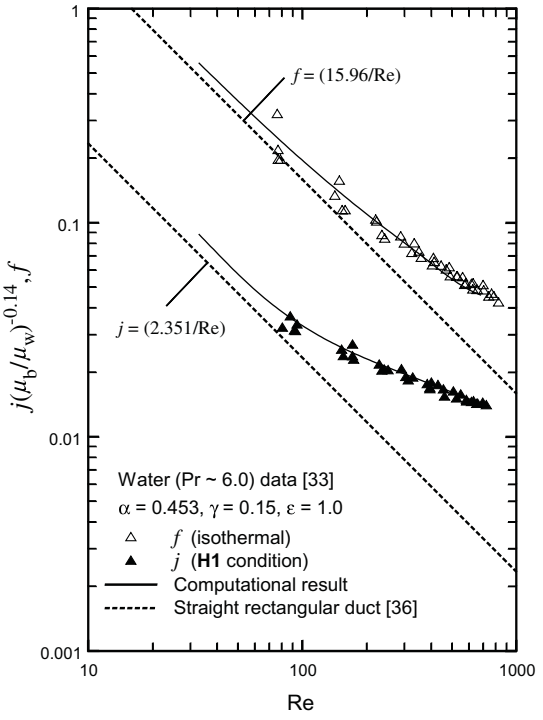

Fig. 2. Comparison of computational results with experimental water data [33] for a sinusoidal wavy channel with $\alpha = 0.453$, $\gamma = 0.15$, $\varepsilon = 1.0$, and uniform heat flux conditions.

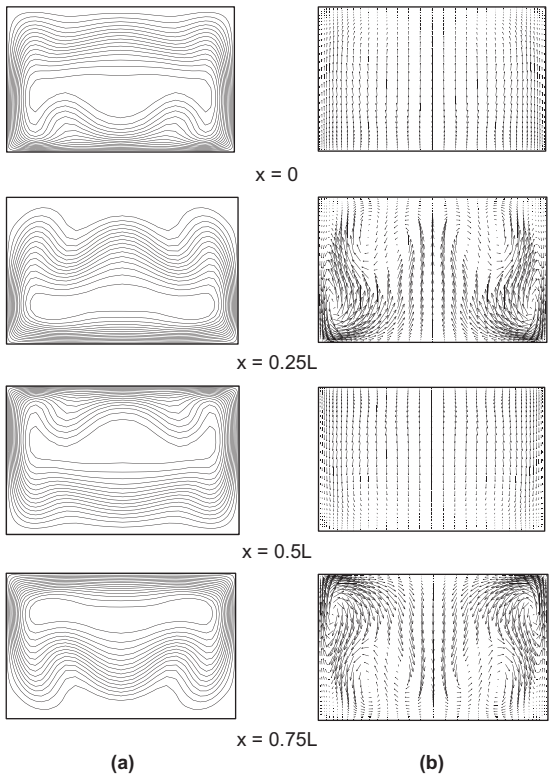

Fig. 3. Velocity distributions in a wavy-fin (Case 2) channel cross-section at different axial locations with $Re = 250$: (a) axial velocity contours, and (b) secondary flow vectors.

exact analytical results [36] of 14.24 and 2.987, respectively. Furthermore, the experimental f and j data reported by Muley et al. [33] for water flows ($Pr \sim 6.0$) in a sinusoidal wavy three-dimensional channel with $\alpha = 0.4533$, $\gamma = 0.15$, and $\varepsilon = 1.0$, and uniform wall heat flux (**H1**) conditions, were found to be in excellent agreement with the computational results as clearly seen in Fig. 2.

4. Results and discussion

Typical flow patterns at different axial locations in a wavy-plate-fin channel module with $\alpha = 0.637$, $\gamma = 0.267$, and $\varepsilon = 0.803$ (Case 2, Table 1) at $Re = 250$ are depicted in Fig. 3. Axial iso-velocity contours and the characteristic secondary velocity distributions in the channel cross-section are presented. The latter is seen to consist of symmetric pairs of counter-rotating vortices that are clustered in a "heart-shaped" formation. Their influence on the axial flow field is evident from the periodic displacement of the accelerating core flow away from the trough region recirculation, and the consequent sharper wall gradients. For a given fin-waviness severity γ, however, the helical recirculation in the wall troughs is also a function of the flow Reynolds number, and this is evident from the secondary flow plots in Fig. 4 for $\gamma = 0.267$ and different Re. Mechanistically, a pair of symmetric helical vortices develops in the valleys or troughs of the wall corrugations as the axial flow separates downstream of the wavy-wall surface peaks. With increasing flow rates, the core flow acceleration breaks up this recirculation into multiple pairs of counter-rotating vortices that dissipate at the subsequent upward curving surface of the next wall peak. The development and steady spatial growth of this swirl flow increases with Re, resulting in greater momentum transport. Also, as flow rates decrease or with very low $Re(\sim 10)$, viscous forces tend to dominate thereby weakening swirl flows.

The impact of swirl flow on the temperature distribution for heat transfer in air flows ($Pr = 0.7$) in the plate-fin geometry with $\alpha = 0.637$, $\gamma = 0.267$, and $\varepsilon = 0.803$ (Case 2; Table 1) is depicted in Fig. 5. Besides reflecting the effects of the two fundamental thermal boundary conditions (**T** and **H1**) on the wavy-fin-channel surface, the local thinning of the thermal boundary layer with sharp wall-temperature gradients, affected by the trough-region helical swirl and core-flow acceleration and its displacement towards the opposite wall, is clearly evident. The enhanced convective heat transport, as the

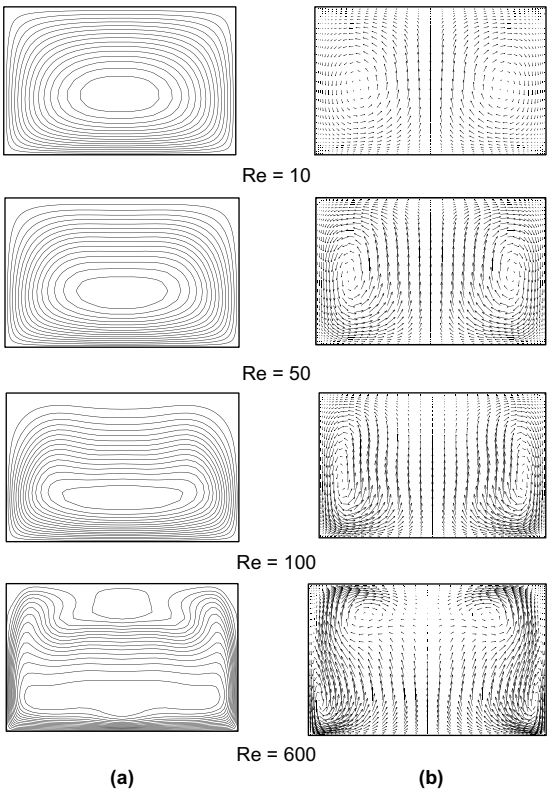

Fig. 4. Variations in the velocity distribution with Re in a wavy-fin (Case 2) channel cross-section at $x = 0.25L$: (a) axial velocity contours, and (b) secondary flow vectors.

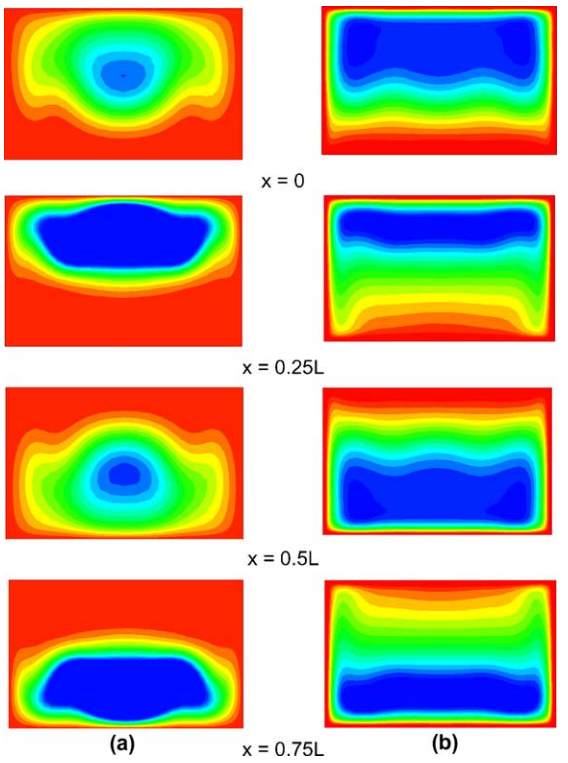

Fig. 5. Temperature distributions for air ($Pr = 0.7$) flow ($Re = 250$) in a wavy-fin (Case 2) channel cross-section at different axial locations with: (a) **T**, and (b) **H1** boundary conditions.

extent of swirl increases with Re in a fixed fin waviness ($\gamma = 0.267$) channel, is further seen from the increasingly sharper wall gradients in the temperature distributions graphed in Fig. 6. Furthermore, as would be expected in confined forced convection with the two boundary conditions, the uniformly heated (or cooled) surface has relatively higher gradients in comparison with those for an isothermal surface.

For a fixed fin height, the spacing ratio ε represents the wavy-fin density and its effects on the velocity and temperature fields are shown in Figs. 7 and 8. For a flow rate with $Re = 500$, axial velocity contours, secondary flow vectors, and isotherm plots in the flow cross-section at the same axial location ($x = 0.25L$) are presented. With increasing fin spacing or decreasing fin density, $\varepsilon = 0.303 \rightarrow 1.22$, the spatial coverage and strength of the counter-rotating vortices is seen to increase (Fig. 7), thereby resulting in considerable convective mixing and enhanced heat and momentum transport. The secondary flow pattern in a large fin-spacing duct ($\varepsilon = 1.22$ and 0.803), however, which consists of two pairs of counter-rotating helical vortices in a heart-shaped pattern, breaks up into three pairs of swirl as ε decreases ($\varepsilon = 0.470$). With higher fin density ($\varepsilon = 0.303$) the spatial swirl coverage diminishes, and a weak recirculation is confined to the side narrow corners of the flow channel. The concomitant impact on the temperature distributions with both the constant wall temperature and heat flux conditions is depicted by the isotherms graphed in Fig. 8 for $Re = 500$, $Pr = 0.7$, and $\varepsilon = 1.22 \rightarrow 0.303$. The transmutation of the thermal field directly reflects the change in vortex structure with ε or fin density. Also evident is the effect of the two boundary conditions, and, as would be expected, locally sharper wall gradients are obtained with **H1** condition in comparison to that with **T**.

Computational results for the period-averaged isothermal Fanning friction and Colburn factors, and their variation with Re for the four cases listed in Table 1 are presented in Fig. 9. The relative f and j values for different fin-spacing ε channels, normalized by their respective straight duct results [36], are graphed. Besides the effects of fin spacing or fin density in the wavy plate-fin core, the onset and growth of surface-curvature induced swirl flows when $Re > 100$ is clearly seen in the sharp slope change of the f–Re and j–Re curves. The increased swirl at higher Re enhances the momentum and heat transport, which increases with fin spacing ($\varepsilon = 0.303 \rightarrow$

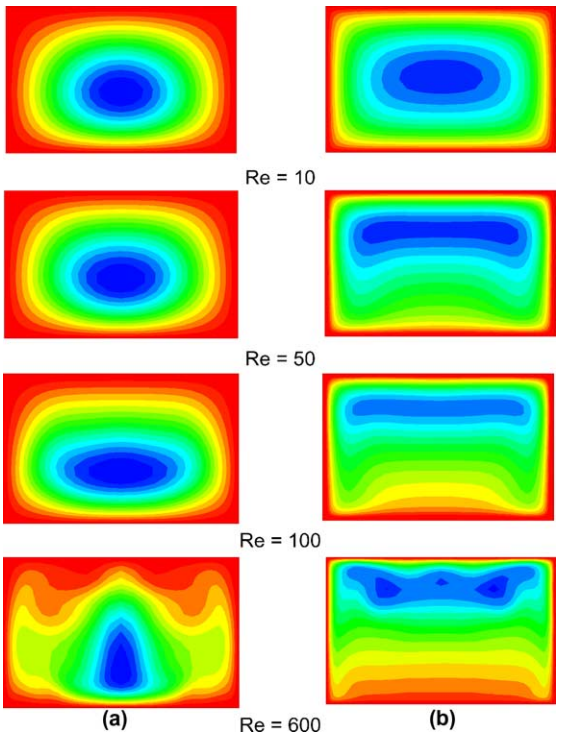

Fig. 6. Variations in the air ($Pr = 0.7$) flow temperature distribution with Re in a wavy-fin (Case 2) channel cross-section at $x = 0.25L$ with: (a) **T**, and (b) **H1** boundary conditions.

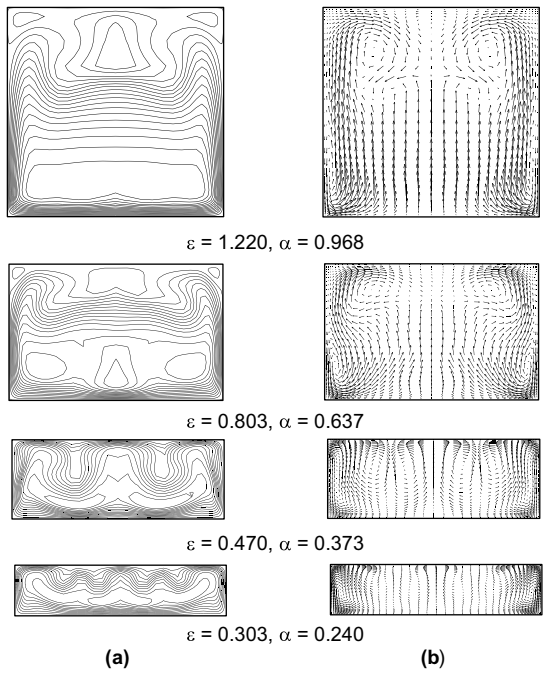

Fig. 7. Velocity field in the flow cross-section at $x = 0.25L$ of different wavy-fin channels with $\gamma = 0.267$ and $Re = 500$: (a) axial velocity contours, and (b) secondary flow.

1.22); in the narrower channel with closer fin spacing, viscous effects tend to dominate. With $Re < 100$, the channel cross-section aspect ratio α has a more significant influence. In a straight rectangular ducts with fully developed laminar flows, as the cross-section varies such that $\alpha = 1 \rightarrow 0$, the isothermal flow friction factor increases as $(fRe) = 14.23 \rightarrow 24$ and, for air flows ($Pr = 0.7$), the heat transfer coefficient increases as $(jRe) = 3.35 \rightarrow 8.49$ with the **T** condition and $4.06 \rightarrow 9.27$ with **H1** [36]. A similar behavior is seen in the performance of wavy plate-fin channels at low Re, though the corresponding f and j are greater (f_{wf}/f_{pf} and $j_{wf}/j_{pf} > 1$) because of the larger surface area and effective flow length (or residence time). Also, a higher thermal performance is obtained with **H1** in comparison to that with the **T** boundary condition.

Considering that both (j_{wf}/j_{pf}) and (f_{wf}/f_{pf}) increase with Re and ε in Fig. 9, it is essential to evaluate the relative enhancement due to the wavy-fin surface and the changing fin density. One way of assessing this thermal-hydraulic performance enhancement, among many other criteria [1,2,4,36], is to consider the *area goodness factor* [36] that can be modified to include flow cross-section aspect ratio effects as follows:

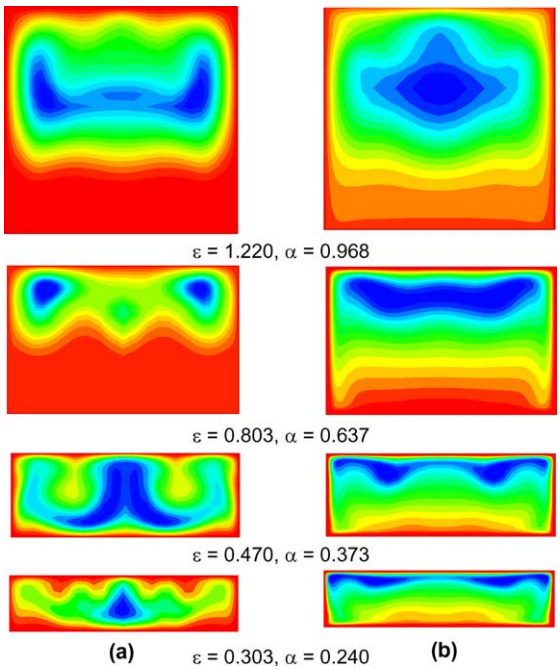

Fig. 8. Temperature field in the flow cross-section at $x = 0.25L$ of different wavy-fin channels with $\gamma = 0.267$ and $Re = 500$: (a) **T**, and (b) **H1** boundary conditions.

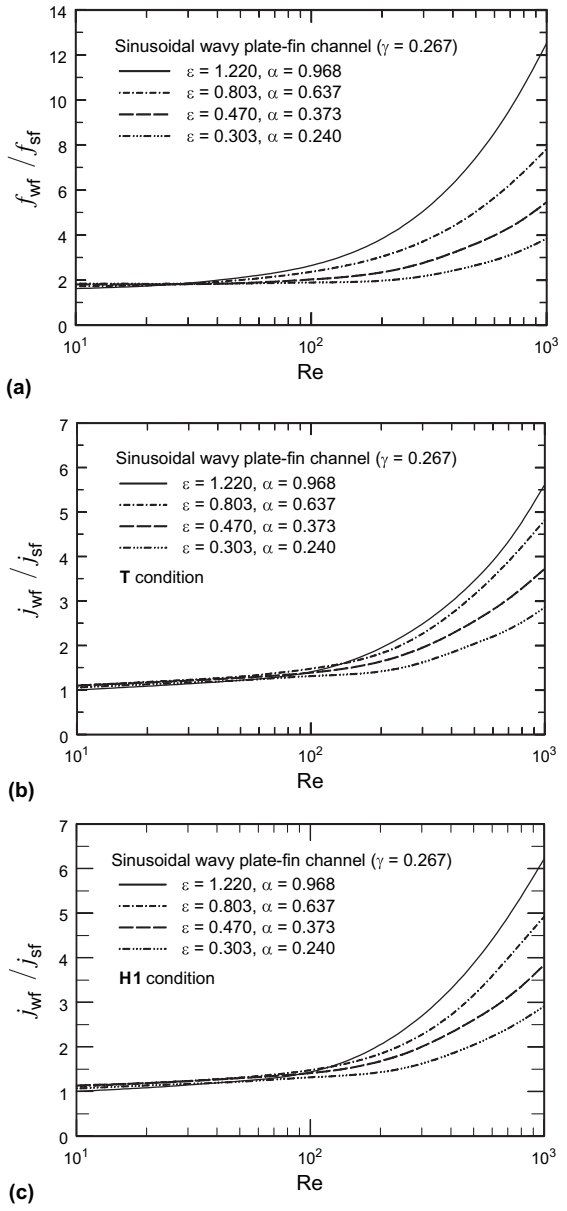

Fig. 9. Thermal-hydraulic performance of wavy-plate fin cores: (a) isothermal f, (b) j for **T** condition, and (c) j for **H1** condition.

$$[(j/f)_{wf}/(j/f)_{sf}] = \left[(NuPr^{-1/3}/fRe)_{wf}/(NuPr^{-1/3}/fRe)_{pf}\right] \quad (12)$$

This criterion seeks to evaluate the free-flow area (and hence the frontal area) requirements of a compact heat exchanger, thereby quantifying the relative compactness of the wavy-surface core. The results for this figure of merit are graphed in Fig. 10, and the influences of Re and ε for a fixed surface waviness ($\gamma = 0.267$) and the two thermal boundary conditions (**T** and **H1**) are clearly

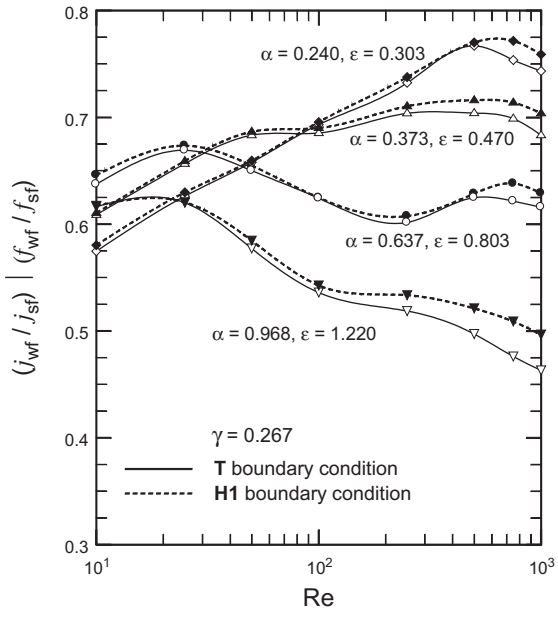

Fig. 10. Enhanced heat transfer performance based on the area goodness factor for wavy-plate-fin cores with different fin density.

evident. In low Re flows ($Re \sim$ O[10]), low fin density or larger ε provides slightly higher enhancement, whereas with higher flow rates ($Re >$ O[100]), or the swirl regime, thermal-hydraulic performance increases with higher fin density (smaller ε). The trade-off between the frictional loss penalty and increased heat transfer coefficients in the swirl regime is seen to provide optimal enhancement with higher density of wavy fins of a given height and waviness, thereby providing greater compactness in wavy-fin heat/mass exchanger cores that are designed for such operating conditions.

5. Conclusions

The computational results presented in this paper provide a detailed understanding of the forced convection behavior in wavy plate-fin channels and the effects of fin density in the steady low Reynolds number regime for air flows ($Pr = 0.7$). The wavy-wall-surface produces a secondary flow pattern that is made up of multiple counter-rotating vortices in flow cross-section of the trough region, and its magnitude and spatial coverage increases with Re and ε. The latter represents wavy-fin density effects, and at low flow rates ($Re < 100$), viscous forces tend to dominate and somewhat suppress or diminish the extent of swirl. Whereas at high Re (>100), the multiple-pair counter-rotating helical swirl promotes higher momentum and convective energy transport. The temperature distributions in the wavy-fin

channel, subjected to either the uniform wall temperature **T** or uniform wall heat flux **H1** boundary condition, correspondingly show a local thinning of the boundary layers with sharper wall gradients; the thermal performance with the **H1** condition, however, is higher than that with the **T** condition. Also, the cross-section aspect ratio α and fin separation ε (α increases with ε for a fixed fin height) appear to have competing effects on the thermal-hydraulic performance, as measured by the surface area goodness factor (j/f) or core compactness, and the optimum dependent upon the flow regime. Nevertheless, increasing fin density (or decreasing ε) tends to promote a relatively better (j/f) performance under swirl-flow conditions and thus provide for a more compact wavy-plate-fin heat exchanger core.

Acknowledgment

This study was supported in part by Honeywell Engines, Systems and Services, University Research Council, and the Thermal-Fluids and Thermal Processing Laboratory.

References

[1] A.E. Bergles, Techniques to enhance heat transfer, in: W.M. Rohsenow, J.P. Hartnett, Y.I. Cho (Eds.), Handbook of Heat Transfer, 3rd ed., McGraw-Hill, New York, 1998, Chapter 11.

[2] W.M. Kays, A.L. London, Compact Heat Exchangers, third ed., McGraw-Hill, New York, 1984.

[3] E.M. Smith, Thermal Design of Heat Exchangers, Wiley, Chichester, UK, 1996.

[4] R.M. Manglik, Heat transfer enhancement, in: A. Bejan, A.D. Kraus (Eds.), Heat Transfer Handbook, Wiley, New York, 2003, Chapter 14.

[5] R.M. Manglik, A.E. Bergles, Heat transfer and pressure drop correlations for the rectangular offset-strip-fin compact heat exchanger, Exp. Thermal Fluid Sci. 10 (2) (1995) 171–180.

[6] R.K. Shah, D.P. Sekulic, Heat exchangers, in: W.M. Rohsenow, J.P. Hartnett, Y.I. Cho (Eds.), Handbook of Heat Transfer, third ed., McGraw-Hill, New York, 1998, Chapter 17.

[7] Y. Asako, M. Faghri, Finite-volume solutions for laminar flow and heat transfer in a corrugated duct, J. Heat Transfer 109 (3) (1987) 627–634.

[8] Y. Asako, H. Nakamura, M. Faghri, Heat transfer and pressure drop characteristic in a corrugated duct with rounded corners, Int. J. Heat Mass Transfer 31 (1988) 1237–1245.

[9] V.K. Garg, P.K. Maji, Flow and heat transfer in a sinusoidally curved channel, Int. J. Eng. Fluid Mech. 1 (3) (1988) 293–319.

[10] L.C. Yang, Y. Asako, Y. Yamaguchi, M. Faghri, Numerical predication of transitional characteristics of flow and heat transfer in a corrugated duct, J. Heat Transfer 119 (1) (1997) 62–69.

[11] T.A. Rush, T.A. Newell, A.M. Jacobi, An experimental study of flow and heat transfer in sinusoidal wavy passages, Int. J. Heat Mass Transfer 42 (9) (1999) 1541–1553.

[12] J. Zhang, J. Kundu, R.M. Manglik, Effect of fin waviness and spacing on the lateral vortex structure and laminar heat transfer in wavy-plate-fin cores, Int. J. Heat Mass Transfer 47 (8-9) (2004) 1719–1730.

[13] C.C. Wang, W.L. Fu, C.T. Chang, Heat transfer and friction characteristics of typical wavy fin-and-tube heat exchangers, Exp. Thermal Fluid Sci. 14 (1997) 174–186.

[14] C.A. McNab, K.N. Heikal, M.R. Heikal, N. Taylor, Numerical modeling of heat transfer and fluid flow over herringbone corrugated fins, Heat Transfer, KSME 6 (1998) 119–124.

[15] J. Min, R.L. Webb, Numerical predications of wavy fin coil performance, in: Proceeding of the 33rd National Heat Transfer Conference, Paper No. NHTC99-168, ASME, New York, 1999.

[16] T. Nishimura, Y. Ohori, Y. Kajimoto, Y. Kawamura, Mass transfer characteristics in a channel with symmetric wavy wall with steady flow, J. Chem. Eng. Jpn. 18 (6) (1985) 550–555.

[17] T. Nishimura, Y. Kajimoto, Y. Kawamura, Mass transfer enhancement in channels with a wavy wall, J. Chem. Eng. Jpn. 19 (2) (1986) 142–144.

[18] W.W. Focke, J. Zachariades, I. Olivier, The effect of the corrugation inclination angle on the thermo-hydraulic performance of plate heat exchangers, Int. J. Heat Mass Transfer 28 (8) (1985) 1469–1479.

[19] C. Zimmerer, P. Gschwind, G. Gaiser, V. Kottke, Comparison of heat and mass transfer in different heat exchanger geometries with corrugated walls, Exp. Thermal Fluid Sci. 26 (2002) 269–273.

[20] H.M. Metwally, R.M. Manglik, Enhanced heat transfer due to curvature-induced lateral vortices in laminar flows in sinusoidal corrugated-plate channels, Int. J. Heat Mass Transfer 47 (10–11) (2004) 2283–2292.

[21] J. Zhang, Numerical simulations of steady low Reynolds number flows and enhanced heat transfer in wavy plate-fin passages, Ph.D. dissertation, Department of Mechanical, Industrial and Nuclear Engineering, University of Cincinnati, 2005.

[22] S. Vyas, J. Zhang, R.M. Manglik, Steady recirculation and laminar forced convection in a sinusoidal wavy channel, J. Heat Transfer 126 (4) (2004) 500.

[23] Y. Asako, M. Faghri, B. Sundén, Three-dimensional laminar forced convection characteristics of wavy ducts with trapezoidal cross section for plate-fin heat exchangers, in: B. Sundén, M. Faghri (Eds.), Computational Simulation in Compact Heat Exchangers, Computational Mechanics, Southampton, UK, 1998, pp. 49–75.

[24] E. Utriainen, B. Sundén, Numerical analysis of primary surface trapezoidal cross wavy duct, Int. J. Numer. Meth. Heat Fluid Flow 10 (6) (2000) 634–648.

[25] E. Utriainen, B. Sundén, A numerical investigation of primary surface rounded cross wavy ducts, Heat Mass Transfer 38 (2002) 537–542.

[26] D.R. Sawyers, M. Sen, H.-C. Chang, Heat transfer enhancement in three-dimensional corrugated channel flow, Int. J. Heat Mass Transfer 41 (1998) 3559–3573.
[27] M. Ciafalo, J. Stasiek, M.W. Collins, Investigation of flow and heat transfer in corrugated passages. II. Numerical simulation, Int. J. Heat Mass Transfer 39 (1) (1996) 165–192.
[28] T. Nishimura, K. Yoshino, Y. Kawamura, Occurrence and structure of Taylor–Goertler vortices induced two-dimensional wavy channels for steady flow, J. Chem. Eng. Jpn. 23 (6) (1990) 697–703.
[29] G. Biswas, K. Torii, D. Fujii, K. Nishino, Numerical and experimental determination of flow structure and heat transfer effects of longitudinal vortices in a channel flow, Int. J. Heat Mass Transfer 39 (16) (1996) 3441–3451.
[30] P. Fang, R.M. Manglik, The influence of inner cylinder rotation on laminar axial flows in eccentric annuli of drilling bore wells, Int. J. Transport Phenomena 4 (4) (2002) 257–274.
[31] A.E. Bergles, R.M. Manglik, Swirl flow heat transfer and pressure drop with twisted-tape inserts, Advances in Heat Transfer, vol. 36, Academic Press, New York, NY, 2002, pp. 183–266.
[32] J. Prusa, L.S. Yao, Numerical solution for fully developed flow in heated curved tubes, J. Fluid Mech. 123 (1982) 503–522.
[33] A. Mulay, J. Borghese, R.M. Manglik, J. Kundu, Experimental and numerical investigation of thermal-hydraulic characteristics of wavy-channel compact heat exchanger-Proc. of the 12th International Heat Transfer Conference, vol. 4, Societe Francaise des Thermiciens and Elsevier, France, 2002, pp. 417–422.
[34] S.V. Patankar, Numerical Heat Transfer and Fluid Flow, Taylor and Francis, New York, NY, 1980.
[35] S.V. Patankar, C.H. Liu, E.M. Sparrow, Fully developed flow and heat transfer in ducts having streamwise-periodic variations of cross-sectional area, J. Heat Transfer 99 (1977) 180–186.
[36] R.K. Shah, A.L. London, Laminar forced convection in ducts, in: T.F. Irvine Jr., J.P. Hartnett (Eds.), Advances in Heat Transfer, Academic Press, New York, NY, 1978, Supplement 1.